An Initial Study on Vehicle Information Extraction from Single Pass QuickBird Satellite Imagery

Zhen Xiong and Yun Zhang

Abstract

Vehicle information is useful in many fields. In this paper, a technique is presented to extract vehicle information from single pass QuickBird images. While passing a target area, the satellite acquires panchromatic (PAN) and multi-spectral (MS) images simultaneously. Because of a small time interval difference between the PAN and MS images, it is theoretically possible to extract two sets of vehicle ground positions from the PAN and MS images, respectively, to identify whether or not a vehicle is in motion, and to calculate the vehicle's velocity and direction. Practically, however, this extraction and calculation are challenging. Since the time interval is very short, a small error in information extraction will result in an unacceptably large error in the calculated vehicle position and velocity. Another challenge is that satellite image pairs (PAN and MS) do not have the same resolution. Therefore, traditional change detection techniques are incapable of providing reliable results, due to varying scales and relief distortions in the co-registered images or slight pixel shifts in the orthorectified images caused by resampling of the PAN and MS images. In order to avoid these errors, this research presents an algorithm through which a vehicle's ground positions can be directly calculated from the raw PAN and MS images. Experiments demonstrate that it is feasible to use this technique to extract vehicle information from high-resolution images obtained from a single satellite pass.

Introduction

Vehicle information (i.e., position, velocity, and direction) is very important for transportation management, security surveillance, and military applications. In order to extract vehicle information, a sequence of vehicle positions is normally acquired in a fixed time interval. These vehicle positions and time intervals are then used to calculate vehicle velocity and direction. The equipment that is usually used for vehicle information extraction includes radar (Liu *et al.*, 2001; Nag *et al.*, 2003; Liu and Jen, 1992), SAR (Dias *et al.*, 2003; Sun *et al.*, 2002; Pettersson, 2004; Soumekh, 2002), and video cameras (Munno *et al.*, 1993). The system platforms are almost always ground-based (Castellano *et al.*, 1999; Nag *et al.*, 2003; Munno *et al.*, 1993; Pettersson, 2004) or aircraft based (Liu *et al.*, 2001; Sun *et al.*, 2002; Soumekh, 2002). To date, satellites have seldom been used.

Radar, SAR, and video cameras can acquire a sequence of images over a relatively long duration (i.e., several seconds to several hours). Each image has the same resolution. Typically the images are registered, and then the vehicle's position change is calculated. Therefore, for Radar, SAR, and video cameras, geometric processing is not a problem. The research focus for such equipment is on automatic target detection and extraction. Some researchers have used a generalized likelihood ratio as a threshold to judge which target is in motion (Liu *et al.*, 2001; Dias *et al.*, 2003; Pettersson, 2004). Others have used a filter (Nag *et al.*, 2003), or have applied a fractional Fourier transformation (Sun *et al.*, 2002) for digital target detection. Munno *et al.*(1993) utilized Victo's frequency domain spatiao-temporal filtering and spatio-temporal constraint error of image frame pairs to detect and track vehicles or people in natural scenes in spite of challenges such as low image contrast, changes in the target's infra-red image pattern, sensor noise, or background clutter (Munno *et al.*, 1993).

The method presented here is completely different, and is based on information obtained from high-resolution imagery provided by a single satellite pass. Some high-resolution satellites such as Ikonos and QuickBird have two sensors. These sensors can therefore acquire two sets of images for the same target area in one pass. For example, the QuickBird satellite can acquire one panchromatic (PAN) image and one multispectral (MS) image in a single pass. The time that the PAN sensor passes through the nadir point is different from that of MS sensor. Therefore, there is a time interval between the PAN image and the MS image (less than one second). If the target vehicle is in motion, the PAN image and MS image will record two different positions of the same vehicle. So theoretically, from a single satellite pass, two different positions of a vehicle can be extracted from the PAN image and MS image, respectively. Thus the vehicle's velocity and direction can be calculated.

This method presents challenges for image processing. First, unlike radar, SAR, and video cameras, QuickBird satellites can only acquire one image pair (a PAN image and a MS image) during each pass, and each image has a different resolution. This makes image registration more difficult than usual. Second, the time interval between the PAN image and MS image is very short. A very small error in

Department of Geodesy & Geomatics Engineering, University of New Brunswick, 15 Dineen Drive, P.O. Box 4400, Fredericton, NB, Canada E3B 5A3 (v009v@unb.ca).

Photogrammetric Engineering & Remote Sensing
Vol. 74, No 11, November 2008, pp. 1401–1411.

0099-1112/08/7411–1401/$3.00/0

registering the vehicle's position will cause a very large error in calculating its velocity. Third, traditional equipment can acquire many images and the vehicle's velocity can therefore be adjusted using the image sequence, but for the QuickBird satellites, only one pair of images can be used to calculate vehicle's position and velocity. Without redundant data, the velocity error is very difficult to find and correct.

Our focus is on how to reduce the error in registering the vehicle's position. Traditionally, the image change detection technique is used for vehicle information extraction. But the accuracy of this technique is directly affected by image scale, ground relief, and image resampling. In order to avoid this problem, a direct location algorithm to calculate vehicle's ground position from its image position based on a Digital Elevation Model (DEM) is developed below.

We believe that this technique offers a new choice for extracting vehicle information. We begin this paper by describing traditional methods and discussing their limitations for use with QuickBird images. We then present our new methodology and test it using QuickBird satellite imagery. Finally, we discuss the results and present our conclusions.

Traditional Methods

Fundamentally there are two different ways to extract vehicle information from images. One is to extract vehicle information in the image domain, and the other is to extract vehicle information in the object domain. These methods use a change detection algorithm to extract the change in the vehicle's position, but as shown below, if these methods are used to process the high-resolution satellite images, there will be many difficulties. These two traditional methods are described in more detail in the following sections, and their limitations for extracting vehicle information from QuickBird satellite imagery are described.

Vehicle Information Extraction in Image Domain (Method 1)

In this method, images are first registered, and then the change detection method is used to extract vehicle's position change. Finally, the vehicle's position, velocity, direction, and acceleration/deceleration are calculated and adjusted (Munno *et al.*, 1993; Nag *et al.*, 2003); Figure 1 shows the flowchart.

After acquiring a sequence of images, the vehicle's speed between two neighboring images can be calculated.

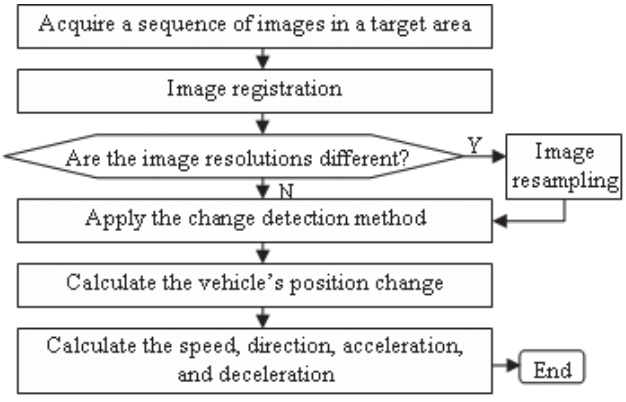

Figure 1. Flowchart of Method 1.

Using this information, the vehicle's acceleration or deceleration can be calculated. From all the vehicle's positions and the time interval, the vehicle's average speed can be calculated (Figure 2).

If this method is applied to QuickBird image pairs, one should first resample the PAN and MS images to the same resolution, then register the resampled images together. Next, one can extract the vehicle's image position from the resampled images. Finally, the vehicle's velocity and direction can be calculated.

For example, if a vehicle moves from point A (I_A, J_A) to point B (I_B, J_B) (Figure 3), in image space, the distance S that vehicle has moved during the time interval is calculated as:

$$S = \sqrt{(I_B - I_A)^2 + (J_B - J_A)^2} \tag{1}$$

where S is distance (pixels), (I_A, J_A) and (I_B, J_B) are image coordinates (pixels); J_A is the column of point A, I_A is the row of point A, J_B is the column of point B, and I_B is the row of point B.

Then, the velocity can be calculated as following:

$$v = \frac{s}{t} \tag{2}$$

where v is speed (pixels/second) and t is time (seconds);

$$\theta = \tan^{-1}\left(\frac{I_B - I_A}{J_B - J_A}\right) \tag{3}$$

where θ is the moving direction angle (degrees) (See Figure 3).

Vehicle Information Extraction in the Object Domain (Method 2)

In this method, the images are first registered, then the PAN and MS images are orthorectified to the same resolution. Next, the change detection method is used to extract

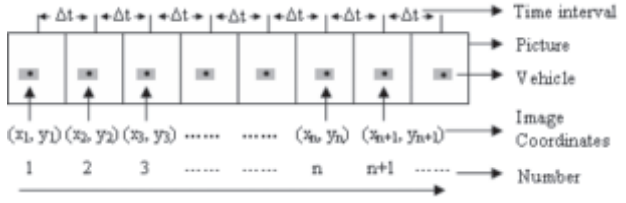

Figure 2. Vehicle information extraction from a sequence of images.

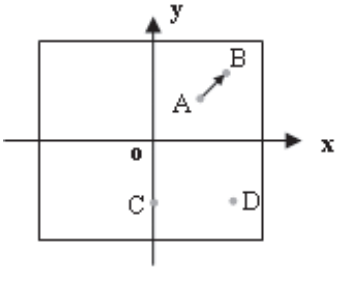

Figure 3. Image specifications (In Image Space, each pixel has a different scale; the nadir point is the smallest pixel.).

the vehicle's position change. Finally, the vehicle's velocity, direction, and acceleration/deceleration are calculated and adjusted. Figure 4 shows the flowchart of Method 2.

The Drawbacks of the Traditional Methods

If Method 1 is used to extract vehicle information from QuickBird images, three factors affect the accuracy of the final result: scale change, ground relief variation, and image resampling error. Because Method 2 includes a process of image orthorectification, it can effectively avoid the error of scale change and ground relief variation, but Method 2 is still affected by the image resampling error. Each of the three types of error is described below.

Scale Change

Before orthorectification, each image pixel on a QuickBird image has a different scale. The nadir point on the image is the smallest pixel. The farther the pixel is from the nadir point, the bigger it is. For QuickBird, the nadir point resolution on the PAN image is 0.61 meters and the 25° off-nadir point resolution is 0.72 meters. The nadir point resolution on the MS image is 2.44 meters and the 25° off-nadir point is 2.88 meters (QuickBird Product Guide, 2003). Therefore, if vehicle C (in Figure 3) moves at a speed of five pixels per second at the nadir point and vehicle D (in Figure 3) also moves at five pixels per second at the off-nadir point, vehicle D is moving faster than vehicle C.

Ground Relief Variation

Before orthorectification, the pixel size on a QuickBird image changes with the ground relief. In Figure 5, from similar triangles ΔLCa and ΔLDA, we can get Equation 4:

$$\frac{Ca}{DA} = \frac{f}{H-h}. \tag{4}$$

From similar triangles ΔLCb and ΔLDB, we can get Equation 5:

$$\frac{Cb}{DB} = \frac{f}{H-h}. \tag{5}$$

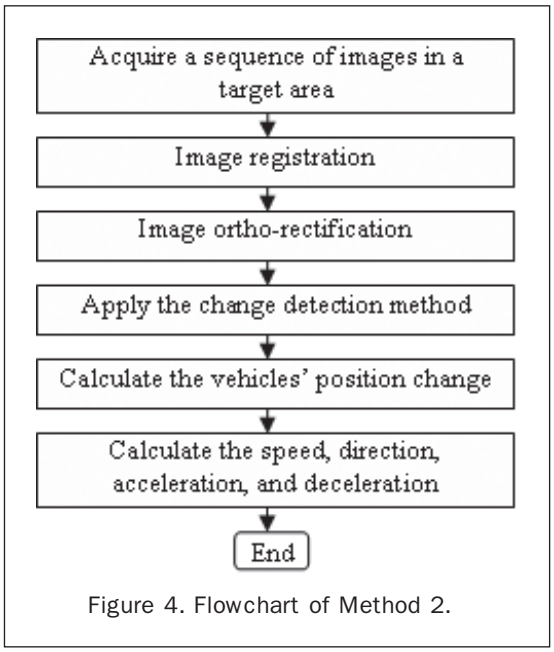

Figure 4. Flowchart of Method 2.

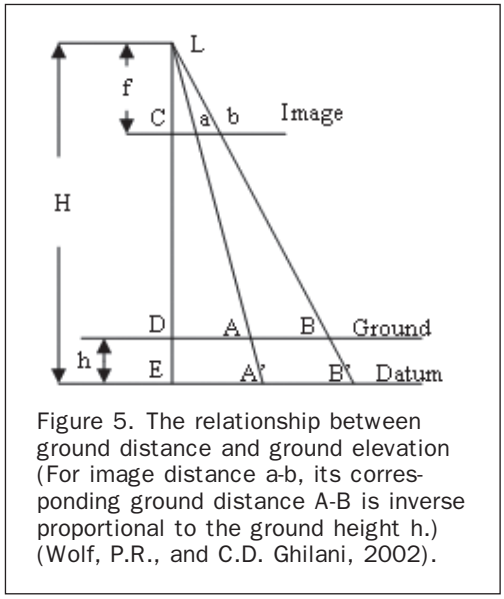

Figure 5. The relationship between ground distance and ground elevation (For image distance a-b, its corresponding ground distance A-B is inverse proportional to the ground height h.) (Wolf, P.R., and C.D. Ghilani, 2002).

From Equation 4 and Equation 5, we can get:

$$\frac{Ca}{DA} = \frac{Cb}{DB} \Rightarrow \frac{Cb}{Ca} = \frac{DB}{DA} \Rightarrow \frac{Cb - Ca}{Ca} = \frac{DB\text{-}DA}{DA} \Rightarrow \frac{ab}{Ca} = \frac{AB}{DA} \tag{6}$$

From Equation 4 and Equation 6, we can get:

$$\frac{ab}{AB} = \frac{Ca}{DA} = \frac{f}{H-h}. \tag{7}$$

From Equation 7, we can get Equation 8:

$$AB = \frac{H-h}{f}ab. \tag{8}$$

For a satellite image, the focal length f and flying height H are constants. For a line ab on the image, its distance AB on the ground is inversely proportional to the ground height h. The greater the ground height h, the smaller the ground distance AB.

Image Resampling Error

Image resampling error can reach 0.5 pixels and directly affects the accuracy of a vehicle's position, velocity and direction. Such an error will result in a 0.3 m position error (for PAN image) and 1.22 m position error (for MS image), respectively.

The Proposed Method for Vehicle Information Extraction

Because the time interval between the PAN and MS images is so small, even a small error in the image position will result in a very large error in the ground position, velocity, and direction. Therefore, every factor that can reduce error and improve accuracy should be considered. In order to avoid the error from image scale, ground relief, and image resampling, a Direct Location Algorithm (DLA) is suggested. This method extracts vehicle information in the object domain, but it does not require image resampling. This method consists of three main components: the DLA, sensor model refinement, and vehicle image position refinement (Figure 6).

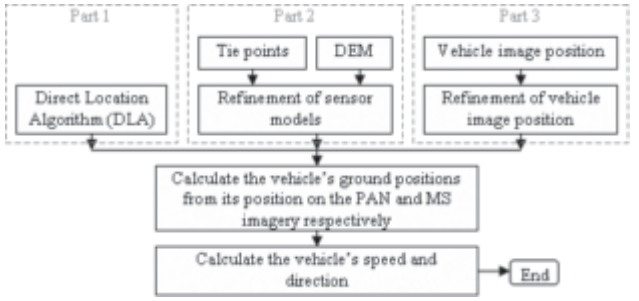

Figure 6. Flowchart of the Proposed Method.

Developing the Direct Location Algorithm (DLA)

In photogrammetry, space intersection can be used to calculate a tie point's ground position. In the current example, this is not feasible. First, the air base is too short (about 7.5 km) compared to the flight height (450 km), and the intersection angle is therefore too small, about two degrees (QuickBird Product Guide, 2003; **http://www.digitalglobe.com**). This means that a small error with an intersection angle will result in very large error in the ground position. Second, the target vehicle is in motion. Therefore, the two points on the PAN and MS images are not tie points. They are actually two different points.

In this research, an algorithm is developed to calculate a vehicle's ground position from its image position based on a DEM. Figure 7 is the flowchart of the DLA.

The steps used to develop this direct location algorithm are described below:

1. From the QuickBird sensor model (RPB), obtain the approximate region (A1, B1, C1, D1) that the image covers (Figure 8). Within this region, select four points (A2, B2, C2, D2) that are near the four corners and obtain the ground position of each corner: A2($X1$, $Y1$), B2($X2$, $Y2$), C2($X3$, $Y3$), and D2($X4$, $Y4$).
2. Interpolate the elevation (Z) of each corner from the DEM. Then, obtain each corner's three-dimensional position: A2($X1$, $Y1$, $Z1$), B2($X2$, $Y2$, $Z2$), C2($X3$, $Y3$, $Z3$), and D2($X4$, $Y4$, $Z4$).
3. Use the sensor model (Equations 12a and 12b) and each corner's ground position (X, Y, Z) to calculate the image position of the four corners: a2($I1$, $J1$), b2($I2$, $J2$), c2($I3$, $J3$), and d2($I4$, $J4$).
4. Use these four points' image coordinates (I, J) and ground coordinates (X, Y, Z) to build a conformal transformation between the image coordinate system and the ground coordinate system:

$$X = f(I, J) = a_1 I + b_1 J + c_1 \quad (9a)$$
$$Y = g(I, J) = a_2 I + b_2 J + c_2 \quad (9b)$$

   where (X, Y) are ground coordinates, and (I, J) are image coordinates.
5. For an image point (I, J), use Equations 9a and 9b to calculate its ground position (X, Y).
6. Then, from (X, Y), each point's height Z is interpolated from the DEM.
7. Then, use the ground position (X, Y, Z) and sensor model (Equations 12a and 12b) to calculate the image coordinates (I', J'). Because the conformal transformation (Equations 9a and 9b) just gives a coarse ground position (X, Y), this position (X, Y) has error. Therefore, the image coordinates (I', J') calculated from this coarse position (X, Y, Z) also contain error and are different from the initial position (I, J).
8. Calculate the difference between these two sets of image coordinates:

$$\Delta I = I - I' \quad (10a)$$
$$\Delta J = J - Jf'. \quad (10b)$$

9. If these differences are less than the threshold, perhaps 0.0001 pixel, stop the iterations and output the ground position (X, Y, Z);
10. Otherwise, use ΔI, ΔJ to correct the ground coordinates (X, Y).

$$\Delta X = a_1 \cdot \Delta I + b_1 \cdot \Delta J \quad (11a)$$
$$\Delta Y = a_2 \cdot \Delta I + b_2 \cdot \Delta J \quad (11b)$$
$$X = X + \Delta X \quad (11c)$$
$$Y = Y + \Delta Y. \quad (11d)$$

11. Go to step 6.

Sensor Model Refinement

Every satellite has a positioning system that can determine each pixel's ground position (on an ellipsoid surface) based on its image position. Each satellite type has a different physical geometric sensor model and different positioning accuracy. Some satellite image vendors, such as SPOT, provide users with a physical sensor model, but others, such as Ikonos and QuickBird, do not because of commercial secrecy. These latter satellite image vendors only release a

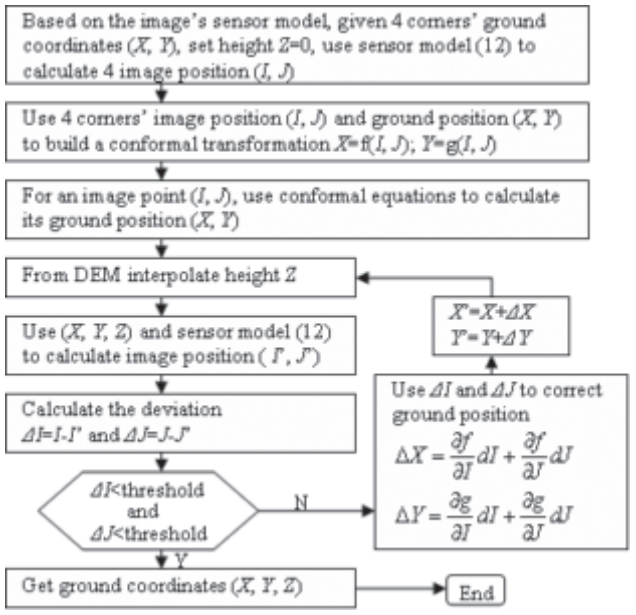

Figure 7. Flowchart of the Direct Location Algorithm.

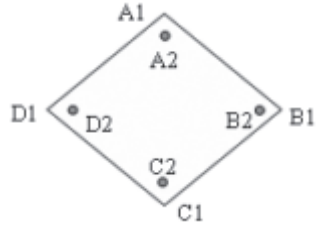

Figure 8. The approximate image region (A1, B1, C1, D1).

rational polynomial coefficient (RPC) as their geometric sensor model, such as the following:

$$\begin{cases} I = \dfrac{P_1(X,Y,Z)}{P_2(X,Y,Z)} & (12a) \\ J = \dfrac{P_3(X,Y,Z)}{P_4(X,Y,Z)} & (12b) \end{cases}$$

$$P(X,Y,Z) = \sum_{i=0}^{m1}\sum_{j=0}^{m2}\sum_{k=0}^{m3} a_{ijk} X^i Y^j Z^k \quad (12c)$$

$$0 \le m_1 \le 3, 0 \le m_2 \le 3, 0 \le m_3 \le 3, m_1+m_2+m_3 \# 3 \quad (12d)$$

where (I, J) are the image coordinates, (X, Y, Z) are the ground coordinates, and a_{ijk} is the polynomial coefficient.

Both the physical sensor model and RPC have a definite value of absolute positioning error. For example, according to the test we conducted, before refinement with ground control points (GCPs), the sensor model provided with SPOT1, SPOT2, and SPOT4 has about a 300-meter absolute positioning error, and the sensor model for SPOT5 has about a 50-meter absolute positioning error. The sensor models for Ikonos and QuickBird each have about a 20-pixel absolute positioning error. If these sensor models are used to calculate a vehicle's ground position, the error of the sensor model will be propagated to the position. Therefore, the sensor model error will affect the final result.

Many researchers have done substantial work on sensor model refinement. Di *et al.* (2003) have proposed two methods to improve the geopositioning accuracy of Ikonos GEO products. One method is to use a large number of GCPs to compute new RPCs. Another method is to use a linear polynomial to correct RPCs in the object domain. Grodeki and Dial (2003) have also proposed the use of a polynomial to correct RPCs in the image or object domain.

Generally, the polynomial correction method can effectively correct the satellite sensor model and provide a relatively good result. For Ikonos imagery, Di *et al.* (2003) improved the ground position accuracy to one to two meters after the sensor model refinement and Grodeki and Dial's results also showed that ground position accuracy had been improved to one to two meters (2003).

In the present research, vehicle velocity and direction are the most important information data to be extracted. Therefore, relative position accuracy is our focus. Other than GCPs, only tie points are used to refine the sensor models. An iteration algorithm was therefore developed to refine the linear polynomial. Finally this polynomial is used to correct the RPCs:

$$\begin{cases} X = a_0 + a_1 X_{RF} + a_2 Y_{RF} + a_3 Z_{RF} & (13a) \\ Y = b_0 + b_1 X_{RF} + b_2 Y_{RF} + b_3 Z_{RF} & (13b) \\ Z = c_0 + c_1 X_{RF} + c_2 Y_{RF} + c_3 Z_{RF} & (13c) \end{cases}$$

where (X, Y, Z) are the ground coordinates after correction, (X_{RF}, Y_{RF}, Z_{RF}) are ground coordinates derived from RPC, and (a_i, b_i, c_i) are correction coefficients. Figure 9 shows the flowchart of sensor model refinement.

The steps used to refine the polynomial coefficients are described below:

1. Use the DLA (Figure 8) to calculate each tie point's ground position. For each tie point, two sets of ground coordinates can be obtained from the PAN and MS images, respectively. They are: $X_{RF}^{(PAN)}$, $Y_{RF}^{(PAN)}$, $Z_{RF}^{(PAN)}$, and $X_{RF}^{(MS)}$, $Y_{RF}^{(MS)}$, $Z_{RF}^{(MS)}$.
2. Calculate the relative deviation between these two sets of ground coordinates. Their average values are used as the final ground coordinates (X, Y, Z) for each tie point.
3. If the biggest relative deviation is less than a threshold ε, stop the iterations and output the polynomial coefficients (a_i, b_i, c_i).

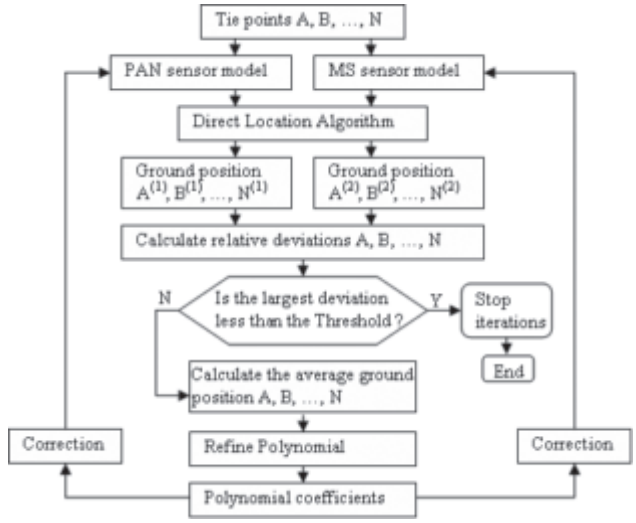

Figure 9. Flowchart of Sensor Model Refinement.

4. A set of average ground positions (X, Y, Z) and the ground positions derived from RPC (X_{RF}, Y_{RF}, Z_{RF}) are used to refine the correction coefficients (a_i, b_i, c_i) in Equation 13.
5. Go to step 1.

Refinement of Vehicle Image Position

Because the vehicle's ground position is calculated from its image position, a "region growing" method is used to refine the vehicle's image position, so as to improve its accuracy. Figure 10 shows the flowchart of the refinement of the vehicle image position.

On a QuickBird image, some long vehicles consist of many pixels (Plate 1a). Normally a vehicle image consists of several pixels (Plate 1b). The problem is to determine which pixel represents the vehicle's central position. Plate 1b shows two vehicles on a QuickBird MS image. One vehicle (A) consists of two pixels, and the other one (B)

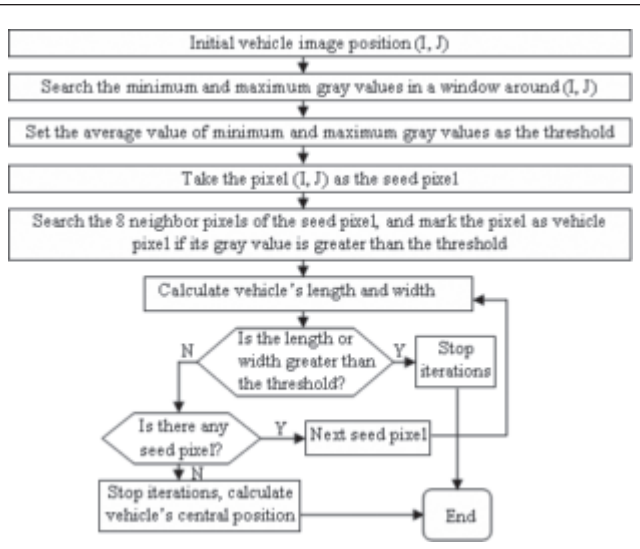

Figure 10. Flowchart of Refinement of Vehicle Image Position.

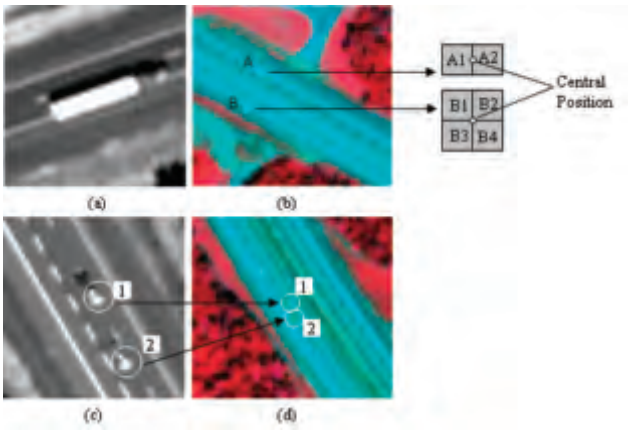

Plate 1. Vehicle Image Position Determination: (a) A long vehicle consists of many pixels, (b) Vehicles consist of several pixels. (A and B are two vehicles on a MS image. A consists of two pixels A1 and A2. B consists of four pixels B1, B2, B3, and B4. The round points represent their central positions.), (c) Two vehicles on the PAN image. (The distance between vehicle 1 and vehicle 2 is just several pixels.), and (d) Two vehicles on the MS image. (The distance between vehicle 1 and vehicle 2 is only one pixel.).

consists of four pixels. Table 1 shows the image position of vehicle pixels and their central image position. Their central positions are (126.5, 552) and (123.5, 560.5), respectively. Obviously, no single pixel can represent the vehicle's central position.

In order to use the vehicle's central image position to calculate its ground position, a "region growing" method is used to collect all the vehicle pixels. The average value of the vehicle's image position is then used as the vehicle's central position.

When the region growing method is used to collect pixels, a threshold should be set up to judge whether or not a pixel represents the vehicle. Here a 5 by 5 window is used for a statistical calculation. The minimum and maximum gray values are searched within this window. The average value of these two gray values is used as the threshold.

TABLE 1. IMAGE COORDINATES OF VEHICLE PIXELS AND VEHICLE CENTRAL POSITION

	Image Coordinates	
Point	Column	Row
A1	126	552
A2	127	552
Central position of point A	126.5	552
B1	123	560
B2	124	560
B3	123	561
B4	124	561
Central position of point B	123.5	560.5

Different vehicles may be in close proximity and, therefore, the vehicle pixels may be overlapping (Plate 1c and 1d). In order to avoid mixing two or more vehicles together, only the connected pixels are considered as belonging to the same vehicle. Some vehicles are very long (Plate 1a), so another threshold corresponding to the long vehicle is used. For example, for a threshold of 20 pixels, if the vehicle length is greater than 20 pixels, then stop region growing and output non-vehicle information.

Test Using QuickBird Images

A pair of level 1A (basic) QuickBird images, which includes a 2.44 meter resolution multispectral image (Plate 2) and a 0.61 meter resolution panchromatic image (Figure 11), was used to test our program. These images were acquired on 26 July 2002 in Gagetown, New Brunswick, Canada. Only a portion of each image was used. Table 2 shows the detailed data clipping information. Because the sensor model RPB is for the whole image, the local image coordinates must include the upper left coordinates of each image before we use the sensor model to calculate a vehicle's ground position from its image position.

The direct location algorithm requires a Digital Elevation Model (DEM) to deliver the third dimension height (Z). In our experiment, a free Global DEM was used, having a resolution of 30 seconds (about 1,000 meters). Figure 12 shows the DEM corresponding to the images, interpolated using a cubic sampling algorithm.

The maximum elevation of this area is 64 meters and the minimum elevation is −5 meters. In the Gagetown area, the elevation of the river water is above mean sea level. Therefore, this DEM has an absolute error of at least 5 meters.

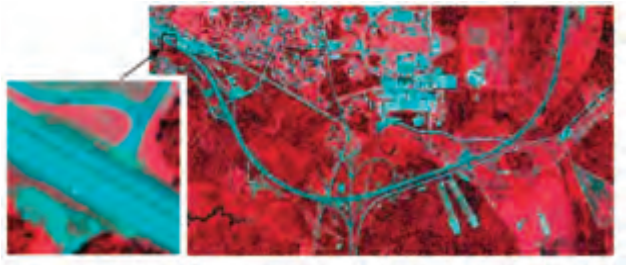

Plate 2. Test Area of QuickBird multispectral image (© DigitalGlobe, 2001, CNES).

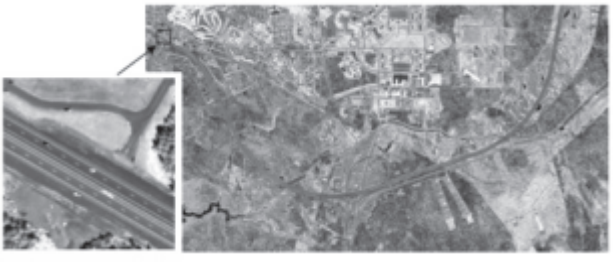

Figure 11. Test area of QuickBird pancromatic image (© DigitalGlobe, 2001, CNES).

TABLE 2. DATA CLIPPING INFORMATION

	MS Data		PAN data	
Point	Column	Row	Column	Row
Upper Left	2865	5047	11200	20000
Lower Right	5937	7007	24000	29000

Because the QuickBird level 1A (Basic) PAN and MS images are not registered, 15 tie points were used to refine the sensor models and register the images together. Table 3 shows image coordinates of the 15 tie points. Table 4 shows the relative position deviation before sensor model refinement, and Table 5 shows the relative position deviation after sensor model refinement. These tables show that after sensor model refinement, the mean deviation of the tie points has been reduced from 3.47 meters to 1.33 meters (Figure 13).

Figure 14 shows 24 vehicles we selected for testing on the panchromatic imagery. Each vehicle's image position was first manually measured. The region growing method was then used to collect all vehicle pixels. Next, these pixels were used to calculate each vehicle's average image coordinates. Table 6 shows each vehicle's initial image coordinates and their final image coordinates after refinement. These refined vehicle image coordinates were then used to calculate their ground coordinates, velocity, and direction. Table 7 shows the result.

Figure 12. Digital elevation model in test area (the minimum height is −5 m and the maximum height is 64 m).

TABLE 3. IMAGE COORDINATES OF TIE POINTS

	MS Image		PAN Image	
No.	Column	Row	Column	Row
1	333	612	1616	1162
2	2730	570	11186	999
3	241	1711	1245	5561
4	2844	1487	11638	4664
5	1333	1778	5608	5827
6	1887	503	7817	730
7	93	506	655	738
8	99	509	681	750
9	91	497	648	702
10	96	500	669	714
11	101	503	689	726
12	94	493	659	687
13	95	490	665	672
14	101	493	687	685
15	106	496	707	696

TABLE 4. GROUND COORDINATES AND RELATIVE DEVIATION OF TIE POINTS BEFORE SENSOR MODEL REFINEMENT

	MS		PAN		
No.	*X*	*Y*	*X*	*Y*	Deviation
1	694451.0	5079302.1	694449.7	5079302.4	1.7
2	700473.8	5079713.1	700472.6	5079712.5	1.7
3	694302.5	5076471.4	694298.9	5076470.2	5.3
4	700826.9	5077380.9	700823.7	5077382.7	5.0
5	697053.7	5076440.0	697052.0	5076441.4	2.6
6	698351.0	5079777.3	698347.8	5079776.3	4.7
7	693837.4	5079541.1	693834.4	5079540.9	4.3
8	693852.8	5079534.2	693851.0	5079534.1	2.4
9	693831.6	5079563.8	693829.2	5079563.7	3.4
10	693844.5	5079556.8	693842.7	5079556.7	2.4
11	693857.3	5079549.8	693855.6	5079549.7	2.4
12	693838.8	5079574.4	693835.9	5079573.6	4.3
13	693841.1	5079582.2	693839.3	5079583.4	2.7
14	693856.5	5079575.3	693853.5	5079575.8	4.2
15	693869.3	5079568.3	693866.3	5079569.5	4.3
Mean Deviation = 3.47 m					

Note: (1) Unit of *X, Y*, and Deviation: Meters.
(2) Coordinate System: UTM WGS84

TABLE 5. GROUND COORDINATES AND RELATIVE DEVIATION OF TIE POINTS AFTER SENSOR MODEL REFINEMENT

	MS		PAN		
No.	*X*	*Y*	*X*	*Y*	Deviation
1	694449.9	5079301.6	694451.0	5079301.8	1.6
2	700472.0	5079712.6	700473.2	5079711.9	1.7
3	694301.4	5076470.8	694300.2	5076469.3	2.3
4	700825.4	5077380.2	700824.2	5077381.8	2.2
5	697052.4	5076439.4	697053.0	5076440.4	1.3
6	698349.5	5079776.8	698348.6	5079775.8	1.6
7	693836.4	5079540.6	693835.8	5079540.5	0.9
8	693851.8	5079533.7	693852.4	5079533.7	0.9
9	693830.6	5079563.4	693830.6	5079563.2	0.1
10	693843.5	5079556.3	693844.1	5079556.3	0.9
11	693856.3	5079549.3	693857.0	5079549.2	0.9
12	693837.9	5079574.0	693837.2	5079573.2	1.1
13	693840.1	5079581.8	693840.7	5079582.9	1.4
14	693855.5	5079574.9	693854.9	5079575.4	0.9
15	693868.3	5079567.9	693867.7	5079569.0	1.4
Mean Deviation = 1.33 m					

Note: (1) Unit of *X, Y*, and Deviation: Meters.
(2) Coordinate System: UTM WGS84

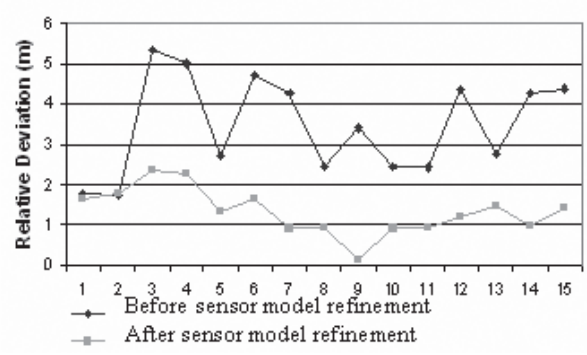

Figure 13. Relative deviation of tie points before and after sensor model refinement.

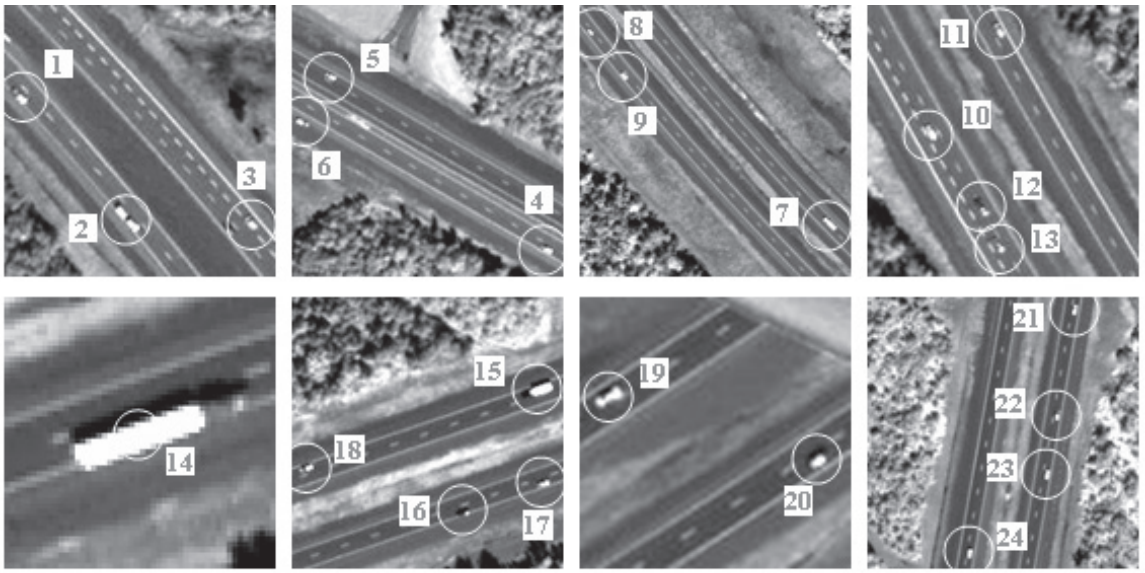

Figure 14. Test Vehicles on PAN Imagery (Each picture has a different scale).

TABLE 6. COORDINATES OF TEST VEHICLES

	Initial Position					After Refinement			
	MS Image		PAN Image			MS Image		PAN Image	
No.	Column	Row	Column	Row	No.	Column	Row	Column	Row
1	331	706	1599	1531	1	330.7	706.3	1599	1531.5
2	345	723	1657	1597	2	344.7	722	1657.1	1596.8
3	358	719	1718	1596	3	357.5	718.5	1718	1596
4	166	583	939	1039	4	165.8	582.6	938.5	1038.6
5	127	552	798	927	5	126.5	552	797.7	926.7
6	124	560	777	955	6	123.5	560.5	776.9	955.3
7	723	1362	3179	4172	7	723	1362.2	3179	4172.3
8	670	1322	2955	3993	8	670.5	1321.5	2955.7	3993.3
9	679	1332	2987	4034	9	678.7	1332.3	2986.9	4034.3
10	608	1230	2707	3626	10	608	1229.5	2707.9	3626.3
11	614	1212	2741	3576	11	614	1212	2740.8	3576.2
12	615	1240	2733	3664	12	615	1239.5	2733.3	3663.9
13	616	1244	2742	3682	13	616	1244	2741.2	3681.8
14	1788	1449	7418	4516	14	1788.7	1449.2	7417.7	4516.2
15	1939	1383	8035	4247	15	1938.8	1383.4	8035	4247.2
16	1933	1400	7991	4320	16	1933	1400	7990.5	4320.5
17	1944	1396	8037	4303	17	1944	1396	8037.6	4302.8
18	1904	1395	7897	4294	18	1904	1395	7896.4	4294
19	2344	1221	9653	3597	19	2344	1221	9652.2	3596.9
20	2365	1224	9717	3617	20	2364.5	1224	9717.4	3616.9
21	2722	579	11151	1044	21	2722.5	578.5	11150.5	1045
22	2719	599	11137	1127	22	2719	599.5	11137.2	1126.7
23	2717	611	11130	1172	23	2716.7	610.7	11129.3	1172.7
24	2701	631	11069	1233	24	2701	631	11069.1	1232.6

Figure 15 shows the position, velocity, and direction of motion of the vehicles.

Table 7 and Figure 15 show that the mean speed is about 100 km/h. We noted that some vehicles were moving at speeds quite different from the mean. We investigated these vehicles in more detail (Table 8). Most of the slow vehicles were found to be either on the road shoulder (vehicle 6) or in the slow lane. In the latter cases, the slow vehicle had either just been passed by another vehicle (vehicle 8 and 15) or was being passed (vehicle 13). For the fast vehicles, they either were passing other vehicles (vehicle 12) or had just passed on other vehicle (vehicle 9 and 18). Some vehicles were in the slow lane, but moving at high speed (vehicles 4, 9, 11, 16, 18, 19, 20, and 22). It is interesting to note that vehicle 24 is in the fast lane, but its speed is only 77.5 km/h. In a real time transportation management or security screening, vehicle 24's speed might be worthy of investigation.

TABLE 7. GROUND COORDINATES, SPEED, AND AZIMUTH ANGLE OF TEST VEHICLES

No.	*X*(m)	*Y*(m)	*H*(m)	Speed(km/h)	Azimuth(°)
1	694447.8	5079066.2	29.5	118.5	133.8
2	694485.7	5079025.9	30.3	109.9	150.1
3	694524.2	5079028.5	30.5	68.1	323.1
4	694021.1	5079358.1	18.0	133.6	126.3
5	693929.8	5079424.8	15.4	93.1	306.8
6	693917.1	5079406.3	15.7	23.8	74.0
7	695493.5	5077424.5	30.5	135.7	317.7
8	695349.1	5077532.0	30.6	113.8	152.4
9	695370.0	5077506.8	30.6	149.7	134.3
10	695185.9	5077759.2	30.3	107.4	150.1
11	695206.4	5077792.3	30.2	145.6	337.5
12	695203.0	5077735.7	30.3	145.4	146.1
13	695209.0	5077724.5	30.3	83.8	164.7
14	698168.0	5077339.5	37.8	71.2	52.9
15	698551.6	5077532.6	43.5	120.4	254.5
16	698525.3	5077484.4	43.6	162.6	74.1
17	698553.9	5077496.8	44.0	127.1	75.3
18	698465.6	5077497.8	42.2	150.2	249.1
19	699557.0	5078000.1	42.4	144.7	243.9
20	699597.5	5077989.3	42.3	143.5	68.1
21	700452.3	5079682.3	27.9	96.3	4.3
22	700445.0	5079628.6	28.1	138.3	11.2
23	700441.4	5079599.5	28.2	100.2	10.3
24	700404.1	5079558.5	28.5	77.5	183.2

Note: (1) Coordinate System: UTM WGS84.
(2) The vehicle's ground position (*X, Y, H*) are derived from its PAN image position.

TABLE 8. VEHICLE INFORMATION EXTRACTED FROM ITS SPEED, POSITION, DIRECTION, AND IMAGE INTERPRETATION

No.	Speed(km/h)	Lane	Note
1	118.5	Slow	
2	109.9	Slow	
3	68.1	Slow	A dark car is passing it
4	133.6	Slow	
5	93.1	Slow	
6	23.8	Shoulder	Parked there
7	135.7	Fast	
8	113.8	Slow	Vehicle 9 just passed it
9	149.7	Slow	Just passed vehicle 8
10	107.4	Slow	
11	145.6	Slow	
12	145.4	Fast	It is passing vehicle 13
13	83.8	Slow	Vehicle 12 is passing it
14	71.2	Slow	Long vehicle
15	120.4	Slow	Vehicle 18 just passed it
16	162.6	Slow	
17	127.1	Slow	
18	150.2	Slow	Just passed vehicle 15
19	144.7	Slow	
20	143.5	Slow	
21	96.3	Slow	
22	138.3	Slow	
23	100.2	Slow	
24	77.5	Fast	Strange !

Error Analysis and Discussion

The accuracy of vehicle information is dependent on the DEM, vehicle image position, the satellite sensor model, and the time interval between capture of the PAN and MS images. The time interval can be considered as constant, since it cannot be changed.

A DEM is used in our method to deliver the third dimension, i.e., height. The DEM's accuracy will directly affect the accuracy of vehicle position. For example, vehicle P's ground position is calculated using its PAN and MS image positions. Then, we can obtain its ground position A. If the DEM has error h, the vehicle's ground position is calculated with height 0, and the vehicle's ground position B and C can then be obtained (Figure 16).

From Figure 16, we can obtain the following equations:

$$S_{PC} = \frac{h}{\cos\alpha} \tag{14}$$

TABLE 9. VEHICLE ERROR CAUSED BY DEM, SATELLITE SENSOR MODEL, AND VEHICLE IMAGE POSITION

	Caused by DEM	Caused by sensor model	Caused by the vehicle's image position (MS)	Caused by the vehicle's image position (PAN)
Error with the vehicle's relative deviation	±0.18 m	±1.33 m	±1.22 m	±0.3 m
Error with the vehicle velocity	±3.31 km/h	±23.94 km/h	±21.96 km/h	±5.4 km/h

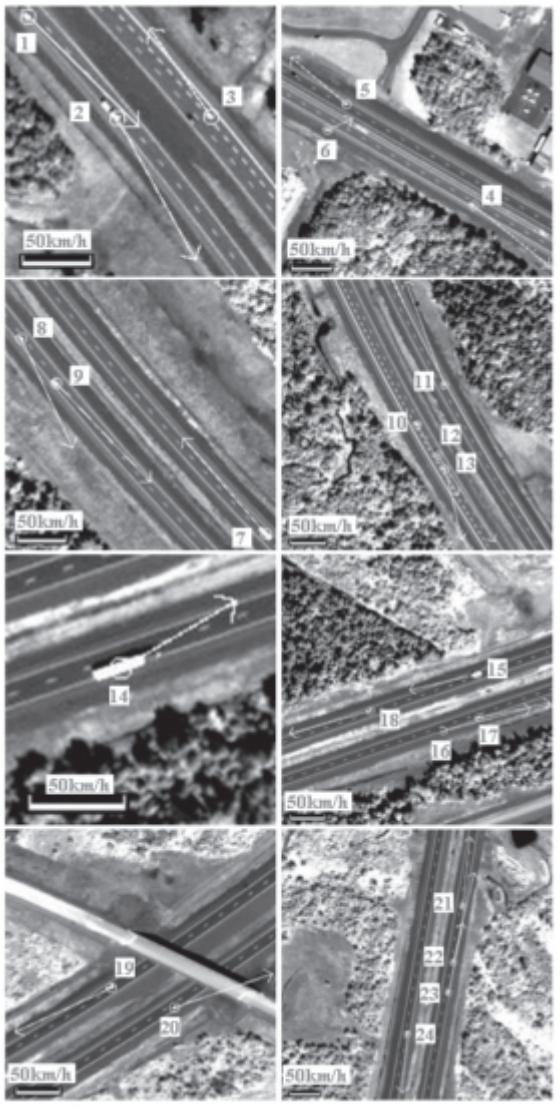

Figure 15. Vehicle velocity and direction extracted from a single pass of QuickBird imagery. Note: Each picture has a different scale, and the arrow length is proportional to the vehicle's speed.

$$S_{AC} = h \cdot \tan\alpha \tag{15}$$

$$S_{BC} = S_{PC} \cdot \varphi \cdot \tag{16}$$

The intersection angle φ (Figure 16) can be calculated from the time interval t, satellite flight speed v, and satellite flight altitude H:

$$\varphi = \frac{vt}{H}? \tag{17}$$

From Equations 16 and 17, we can get Equation 18:

$$S_{BC} = \frac{h}{\cos\alpha} \cdot \frac{vt}{H} \tag{18}$$

where S_{AC} is the vehicle's position error caused by DEM error, and S_{BC} is the relative deviation caused by the DEM error. In this experiment, a Global DEM with a resolution of 30 seconds was used. We assume that the error of this DEM is 10-meters. Here, if the incidence angle is 25 degrees and intersection angle is one degree, then the position error will be 4.66 m and relative deviation will be 0.18 m. Obviously, the position error is much greater than the relative deviation. Because it is the relative deviation, not the ground position that directly affects the vehicle's velocity calculation, the

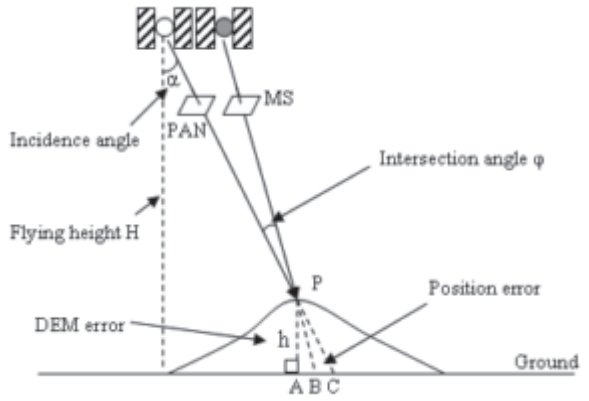

Figure 16. Position error caused by DEM error. DEM error "h" will result in ground position error A-B (when calculated from MS image position) and A-C (when calculated from PAN image position).

effect of DEM error on the vehicle's ground position is much more severe than that of the vehicle's velocity.

Besides the DEM, another factor that affects the accuracy of the vehicle position is the satellite sensor model. In our method, a linear polynomial was used to correct the sensor model. After refinement, the mean relative deviation of tie points was reduced from 3.47 m to 1.33 m.

The third factor affecting accuracy is the vehicle's image position. If the vehicle's image position has a 0.5 pixel error, the vehicle's ground position will be 0.3-meters (for the PAN image) and 1.22-meters (for the MS image). Although a region growing method is used to collect all the vehicle pixels and all these pixels are used to calculate the vehicle's central position because a threshold for image segmentation is used to judge whether a pixel is a vehicle or not, the image segmentation is pixel accuracy. If a sub-pixel segmentation method is used here, the accuracy of the vehicle image position will be improved.

Table 9 shows the vehicle's error caused by DEM, satellite sensor model, and the vehicle's image position. Compared these three error sources, it is very obvious that the vehicle error mainly comes from the satellite sensor model, and the vehicle image position, especially the vehicle image position on the MS image. The DEM error contributes the smallest part to the vehicle error.

Conclusions

A new method of vehicle information extraction from a single pass of QuickBird imagery is presented. It includes three major components: (a) A new approach using tie points to refine sensor models, (b) a method to refine vehicle's image position, and (c) a new direct location algorithm to calculate a vehicle's ground position from its image position. The experimental results show that this technique can effectively extract a vehicle's position, velocity, and direction. Most of the high-resolution satellites can now acquire both PAN and MS images. So this technique potentially offers a new cost-effective choice to extract vehicle information.

We also recognize that there is still potential for further improvement in the vehicle image coordinates calculation and sensor model refinement. A more precise DEM is another way to improve the accuracy. Because the satellite time interval is very small, even a marginal improvement in the vehicle image coordinates, say 0.1-pixel, will yield a very large contribution to the accuracy of vehicle information. This will be the focus of our future research.

References

Castellano, G., J. Boyce, and M. Sandler, 1999. CDWT optical flow applied to moving target detection, *IEEE Colloquium on Motion Analysis and Tracking* (Ref. No. 1999/103), 10 May, pp. 17/1–17/6.

Di, K.R. Ma, and R. Li, 2003. Rational functions and potential for rigorous sensor model recovery, *Photogrammetric Engineering & Remote Sensing*, 69(1):33–41.

Dias, J.M.B., and P.A.C. Marques, 2003. Multiple moving target detection and trajectory estimation using a single SAR sensor, *IEEE Transactions on Aerospace and Electronic Systems*, 39(2):604–624.

Grodecki J., and G. Dial, 2003. Block adjustment of high-resolution satellite images described by rational polynomials, *Photogrammetric Engineering & Remote Sensing*, 69(1):59–68.

Liu, C.-M. and C.-W. Jen,1992. A parallel adaptive algorithm for moving target detection and its VLSI array realization, *Signal Processing, IEEE Transactions on Acoustics, Speech, and Signal Processing*, 40(11):2841–2848.

Liu, G., and J. Li, 2001. Moving target detection via airborne HRR phased array radar, *IEEE Transactions on Aerospace and Electronic Systems*, 37(3):914–924.

Munno, C.J., H. Turk, J.L. Wayman, J.M. Libert, and T.J. Tsao, 1993. Automatic video image moving target detection for wide area surveillance, *Security Technology Proceedings, Institute of Electrical and Electronics Engineers 1993 International Carnahan Conference*, 13–15 October, pp. 47–57.

Nag, S., and M. Barnes, 2003. A moving target detection filter for an ultra-wideband radar, *Proceedings of the IEEE Radar Conference 2003*, 05–08 May, pp. 147–153.

Pettersson, M.I., 2004. Detection of moving targets in wideband SAR, *IEEE Transactions on Aerospace and Electronic Systems*, July, 40(3):780–796.

Reed, I.S., R.M. Gagliardi, and L.B. Stotts, 1988. Optical moving target detection with 3-D matched filtering, *IEEE Transactions on Aerospace and Electronic Systems*, July, 24(4):327–336.

Soumekh, M., 2002. Moving target detection and imaging using an X band along-track monopulse SAR, *IEEE Transactions on Aerospace and Electronic Systems*, January, 38(1):315–333.

Sun, H., G. Liu, H. Gu, and W. Su, 2002. Application of the fractional Fourier transform to moving target detection in airborne SAR, *IEEE Transactions on Aerospace and Electronic Systems*, October, 38(4):1416–1424.

Wolf, P.R., and C.D. Ghilani, 2002. *Elementary Surveying: An Introduction to Geomatics*, Tenth edition.

(Received 18 January 2006; accepted 10 January 2007; revised 28 March 2007)